https://doi.org/10.5194/tc-2019-106
Preprint. Discussion started: 29 May 2019

The Cryosphere Discussions
Open Access
EGU

Evaluating continuous and autonomous snow water equivalent measurements by a cosmic ray sensor on a Swiss glacier

Rebecca Gugerli[1], Nadine Salzmann[1], Matthias Huss[1,2], and Darin Desilets[3]

[1]Department of Geosciences, University of Fribourg, Fribourg, Switzerland
[2]Laboratory of Hydraulics, Hydrology and Glaciology (VAW), ETH Zurich, Zurich, Switzerland
[3]Hydroinnova LLC, Albuquerque, NM, USA

Correspondence: Rebecca Gugerli (rebecca.gugerli@unifr.ch)

Abstract. Snow water equivalent (SWE) measurements are crucial in many research fields. Yet accurate measurements at a high temporal resolution are difficult to obtain in high mountain regions. With a cosmic ray sensor (CRS), SWE can be directly derived from neutron counts. In this study, we present the analyses of temporally continuous SWE measurements by a CRS on a Swiss glacier (Glacier de la Plaine Morte) over two winter seasons (2016/17 and 2017/18), which were markedly different in terms of amount and timing of snow accumulation. By combining the SWE values with snow depth measurements, we calculate the daily mean density of the snowpack. The autonomous measurements overestimate SWE by +2%±12% compared to manual field observations (snow pits). Snow depth and mean density agree with manual in situ measurements with a standard deviation of ±6% and ±8%, respectively. In general, the cosmic ray sensor measured with high reliability during these two winter seasons and is, thus, considered an effective method to measure SWE at remote high alpine sites. We use the daily observations to break down the winter season into days either dominated by accumulation (solid precipitation, snow drift), ablation (snow drift, melt) or snow densification. The prevailing meteorological conditions of these periods are clearly distinct for each of the classified processes. Moreover, we compare daily SWE amounts to precipitation sums from three nearby weather stations located at lower elevations, and to a gridded precipitation dataset. We determine the best-possible scaling factor for these precipitation estimates in order to reproduce the measured accumulation on the glacier. Using only one scaling factor for the whole time series, we find a mean absolute error of less than 8 cm w.e. for the reproduced snow accumulation. By applying temperature-specific scaling factors, this mean absolute error can be reduced to less than 6 cm w.e. for all stations.

1 Introduction

The annual amount of snow accumulation in high mountain regions is a key parameter in many climate-related research fields such as glaciology or hydrology and climate change impacts, risks and adaptation. Changes in snow accumulation in mountain areas caused by climate change are expected to have major impacts on water supply for adjacent lowlands (Barnett et al., 2005; Viviroli et al., 2007, 2011), hydropower production (Ali et al., 2018) or winter tourism (Marty et al., 2014; Sturm et al., 2017). In addition, information of the amount of water stored within the annual snowpack (snow water equivalent, SWE) in high mountain regions is crucial for avalanche prediction (Castebrunet et al., 2014), flood prevention (Jörg-Hess et al., 2015), or mass balance calculations of glaciers (Sold et al., 2013; Pulwicki et al., 2018). Despite the high demand for accurate SWE

https://doi.org/10.5194/tc-2019-106
Preprint. Discussion started: 29 May 2019

measurements in high mountain regions, reliable and temporally continuous measurements of SWE are still difficult to obtain. Mostly, the cold and windy conditions pose the main challenge for accurate measurements (Sevruk et al., 2009; Rasmussen et al., 2012; Kinar and Pomeroy, 2015).

Manual in situ field measurements with snow pits and snow probes usually provide reliable data. Nevertheless, they are not suited for continuous measurements because they are invasive, laborious, and logistically complicated for remote sites. Various devices to measure snow accumulation autonomously and continuously at high elevations have been tested and applied during the past decades (Pirazzini et al., 2018). However, the uncertainty of these devices remains high. For example, snow gauges are known to carry large uncertainties in the extreme environments of high mountains through undercatch and post-event thawing (e.g. Goodison et al., 1998; Rasmussen et al., 2012; Martinaitis et al., 2015). Snow pillows (and snow scales) are rarely suitable in high mountain regions because they require a large flat surface (e.g. Egli et al., 2009; Kinar and Pomeroy, 2015). In addition, ice bridging can falsify the measurements (e.g. Sorteberg et al., 2001; Johnson and Schaefer, 2002). Ground-penetrating radar (GPR) is another method to determine snow accumulation and has been used in various studies (e.g. Heilig et al., 2009, 2010). Schmid et al. (2014) combine a snow depth (SD) sensor with an upward looking GPR (upGPR) installed within the ground below the snowpack. This combination results in continuous estimates of liquid water content, SD and SWE at a high temporal resolution. SWE derived from this method lies within $\pm 5\%$ discrepancy from manual measurements. In a follow-up study, Schmid et al. (2015) combined an operational upGPR with a low-cost GPS to render the approach independent from additional sensors (e.g. SD). Despite the good agreement with manual measurements of SWE, the underlying algorithm to derive SWE from the upGPR is still prone to errors. For instance, a deviation of 10% in SD may lead to an over- or underestimation of 30-40% of the resulting SWE (Schmid et al., 2014). Furthermore, erroneous identifications of the reflection horizons affect the resulting SWE (Heilig et al., 2009; Schmid et al., 2015). Steiner et al. (2018) present sub-snow GPS as a method to continuously monitor snow accumulation. Data processing of the GPS signals is elaborate.

Other approaches use empirically derived or physically calculated bulk snow densities to calculate the SWE from continuous SD measurements. The approach presented by Jonas et al. (2009), for instance, uses automatic measurements of SD with an empirically derived model to estimate the bulk snow density in various regions of the Swiss Alps for different elevations and months. The model agreement to manual measurements lies within the site variability of snow density and SWE. However, Jonas et al. (2009) state that the model may not be suitable for daily or sub-daily SD measurements. A physically-based model in operational use is, for instance, the model SNOWPACK (Lehning et al., 1999). The Swiss Federal Institute for Snow and Avalanche Research runs this model with data from high-elevation weather stations to derive snow properties for avalanche forecasting (Lehning et al., 1999). In general, Raleigh and Small (2017) show that 75% of the uncertainty of estimated SWE is caused by the uncertainty of modeled snow density. In their study, they observed SD with an airborne lidar and modeled snow density with four different models (two empirically based and two physically based).

The cosmic ray sensor (CRS) is a re-discovered method to measure snow accumulation continuously. A CRS counts the number of fast neutrons, which originate from the interaction of cosmic rays with various nuclei within the Earth's atmosphere. When these neutrons arrive at the Earth's surface, hydrogen atoms easily moderated them. Thus, the number of neutrons is negatively correlated to the number of hydrogen atoms present in the vicinity and allow inferring the SWE (Zreda et al.,

https://doi.org/10.5194/tc-2019-106
Preprint. Discussion started: 29 May 2019

2008; Desilets et al., 2010). The CRS has first been deployed by Kodama et al. (1975) and Kodama (1980) in the 70s and already showed promising results with an error of less than 7% for cosmic-ray-derived SWE measurements compared to manual measurements. Almost 20 years later, the French Electric Utility developed their own CRS and integrated these in a mountain monitoring network in order to manage hydroelectric power (Paquet and Laval, 2005; Paquet et al., 2008). In 2013, this monitoring network counted 37 sites in the French Alps and the Pyrenees (Gottardi et al., 2013). These CRS are all installed below the snowpack. More recent studies have investigated the potential of SWE measurements with above-ground CRS, which provide a larger footprint of 230-300 m (Sigouin and Si, 2016; Schattan et al., 2017). Independently of the sensor's deployment above or below the snowpack, the SWE measurements were influenced by changes in soil moisture through snow melt (Kodama, 1980; Paquet and Laval, 2005; Sigouin and Si, 2016). A shield was thus added to the CRS to prevent influences from increases in soil moisture from the surrounding ground (Paquet and Laval, 2005). Schattan et al. (2017) state that this effect is negligible for deep snowpacks. Nevertheless, these influences can be almost entirely avoided by placing the CRS on an ice surface such as a polar ice sheet or a mountain glacier. In the recent study by Howat et al. (2018), the CRS was deployed below the snowpack on the Greenland Ice Sheet. With almost 24 months of measurements, they find an instrument precision of approximately 0.7% and a good agreement with manual measurements.

In this study, we evaluate the applicability of the CRS for continuous SWE measurement on Glacier de la Plaine Morte in the Swiss Alps, including a rigorous uncertainty analysis. On the given glacier site (2690 masl), we have a generally lower neutron count than in the study by Howat et al. (2018) which is at 3216 masl. This is due to the lower latitude and elevation. Moreover, the combination with continuous SD measurements allows the calculation of the bulk snow density at a daily resolution. With the daily density values, we analyze the temporal evolution of the bulk snow density over two winter seasons. Furthermore, we analyse the general processes within the snowpack by applying criteria to daily changes in SD and SWE. Thereby, we identify the days that are dominated by accumulation, ablation, and densification. For each of these process-classified days we investigate their prevailing meteorological conditions.

In a second application, we aim at reproducing snow accumulation by using precipitation estimates from nearby stations at lower elevations. Because automatic and continuous estimates of precipitation are even more challenging to obtain in high mountain regions, considerable uncertainties are introduced in many mountain precipitation climatologies (e.g. Efthymiadis et al., 2006; Isotta et al., 2014, 2019). Nonetheless, such precipitation data are useful. One application is, for example, the operational evaluation of winter mass balance on Swiss glaciers (GLAMOS, 1881-2018). Based on scaling daily precipitation to observed end-of-season measurements of SWE, the temporal evolution of mass balance is inferred (see e.g. Huss et al., 2009, 2015; Sold et al., 2016). In the case of Plaine Morte and its mass balance monitoring, for instance, precipitation amounts are currently taken from the Montana weather station, which is in the vicinity of the glacier (Huss et al., 2013; GLAMOS, 1881-2018). Given the continuous observations of SWE, we evaluate the application of a constant scaling factor on the precipitation observations to reproduce snow accumulation on the glacier. In a simple approach, we use only one scaling factor on a selection of weather stations and gridded precipitation data. In a more elaborate approach, we define three different scaling factor for each weather stations. The three scaling factors depend on the hourly air temperature on the glacier.

https://doi.org/10.5194/tc-2019-106
Preprint. Discussion started: 29 May 2019

The Cryosphere
Discussions
Open Access
EGU

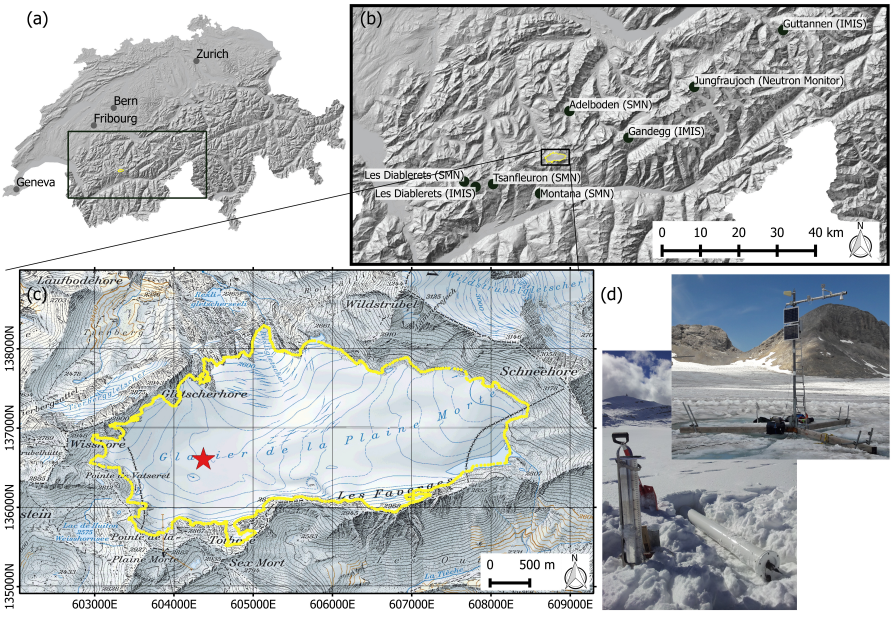

Figure 1. (a) Map of Switzerland. (b) Map of the excerpt marked in (a), and all weather stations used in this study (black dots). (c) Topographic map of Plaine Morte with the red star indicating the location of the AWS with the CRS (see (d)). The yellow contour represents the current outline of Plaine Morte (Fischer et al., 2014). The coordinates correspond to the Swiss coordinate system (CH1903). (Maps provided by Swisstopo).

2 Study site

Our study site is located on the Glacier de la Plaine Morte (in the following: Plaine Morte), where we deployed a CRS along with an automatic weather station. This glacier is situated on the ridge between two Alpine regions of Switzerland, the Bernese Alps in the North and the Rhône valley in the South (Huss et al., 2013).

Plaine Morte is particular in that it has almost no elevation gradient. With a surface area of 7.4 km^2 it is the largest plateau glacier in the European Alps. Due to its flatness, the equilibrium line is located either above or below the glacier surface, rendering it completely snow-free or snow-covered at the end of summer, respectively. For the same reason, the winter snow distribution shows only small spatial variability (Huss et al., 2013; GLAMOS, 2018).

Since its integration in the glacier monitoring network of Switzerland in 2009, the annual mass balance has been negative with an average loss of 1.4 m w.e. per year. This is despite a mean winter gain between 2009 and 2017 of 1.3±0.2 m w.e. (GLAMOS, 1881-2018).

https://doi.org/10.5194/tc-2019-106
Preprint. Discussion started: 29 May 2019

Table 1. Sensors used in this study.

Name	Distributor	Parameter
CNR4	Kipp & Zonen	shortwave radiation
CS215	Campbell Scientific	air temperature, relative humidity
UMB Ventus	Lufft	air pressure, wind speed, wind direction
SnowFox^{TM} (CRS)	Hydroinnova	snow water equivalent (fast neutrons)
SR50A	Campbell scientific	snow depth

3 Data

In October 2016, we installed an automatic weather station on Plaine Morte (2690 masl, Fig. 1) with sensors to measure SD, air temperature, humidity, air pressure and shortwave radiation (the latter only added in October 2017). The CRS (SnowFox^{TM} provided by Hydroinnova) is also connected to the station. We have conducted 11 field campaigns over two winter seasons to measure SD and SWE manually. Additionally, we use observational and gridded meteorological data provided by the Federal Office of Meteorology and Climatology (MeteoSwiss) for comparison and for best-possible data completion. All data are described below in detail.

3.1 Automatic weather stations

We have installed a five meter high mast on the bare ice of Plaine Morte on which we mounted all sensors (see Table 1) at 4.8 m height above the glacier surface. These sensors measured continuously at an hourly interval during two winter seasons (20 October 2016 to 29 July 2018). The CRS lies on the bare ice, i.e. below the snowpack, at approximately 8 m horizontal distance from the mast to avoid any impacts caused by potential maintenance work.

Precipitation data for comparison to snow accumulation are taken from the federal network of weather stations in Switzerland (SwissMetNet, Table 2). The stations are selected according to data quality and the geographic location relative to Plaine Morte. Next to the SwissMetNet stations, we also considered stations equipped with a pluviometer from the high-elevation weather station network in the Swiss Alps (IMIS, intercantonal measurement and information system, SLF Data, 2015). However, precipitation observations of selected stations had long data gaps during winter and could therefore not be used.

For further comparison, we used gridded precipitation from the RhiresD product (MeteoSwiss, 2013). This product uses rain-gauge measurements which are spatially analysed and pre-processed and then interpolated to a 1×1 km grid at daily resolution covering the Swiss territory (MeteoSwiss, 2013). From this dataset we extract time series of the three grid points closest to the position of the CRS.

https://doi.org/10.5194/tc-2019-106
Preprint. Discussion started: 29 May 2019

Table 2. Table with three meteorological stations with precipitation measurements and three grid cells of the gridded precipitation. For the gridded precipitation, the coordinate represents the centers of the corresponding pixel.

Station name	Coordinates (CH-1903)	Elevation [masl]	Source
Adelboden	609350/ 149001	1322	SwissMetNet
Montana	601709/ 127488	1427	SwissMetNet
Tsanfleuron	589461/ 129932	2052	SwissMetNet
grid cell 1 (1km^2)	605500/ 136500	2299	RhiresD
grid cell 2 (1km^2)	604500/ 136500	2579	RhiresD
grid cell 3 (1km^2)	604500/ 137500	2579	RhiresD

3.2 Field data

Over the two winter seasons 2016/17 and 2017/18, we conducted 11 field campaigns to obtain data for comparison. During two of these campaigns (20 October 2016 and 5 December 2017), we installed the CRS. Because of the disturbed snowpack, the measurements of these two campaigns are only used to account for the already existing SWE on the glacier.

During the field campaigns, we measured SWE by means of snow pits and snow tube sampling (e.g. Cogley et al., 2011; Kinar and Pomeroy, 2015) and SD with snow probes. The snow pits were dug in the vicinity of the station, but each time at a different location to avoid sampling a disturbed snowpack.

4 Methods

4.1 Filling measurement gaps

The measurement period considered in this study covers two continuous but highly distinctive winter seasons (20 October 2016 to 29 July 2018). During summer 2017, the weather station on Plaine Morte only measured wind, temperature and relative humidity. In winter 2017/18, unusually high amounts of snow buried most of the mast causing several interruptions of measurements. The time spans of the data gaps differ for the sensors because of their measurement characteristics. The SD sensors, for instance, requires a minimal distance of 0.5 m to the target surface (Campbell Scientific, 2016) and thus has the longest data gap. Another issue was the power consumption of the station since the solar panels were buried, too. To conserve energy, we turned off the heated wind sensor (highest energy consumption), which measures wind speed, wind direction, and air pressure. Furthermore, we did not consider wind speed, temperature and relative humidity from 10 March 2018 to 17 April 2018 because of the proximity of the sensors to the snow surface.

https://doi.org/10.5194/tc-2019-106
Preprint. Discussion started: 29 May 2019

Once deployed, the CRS measured reliably over the two winter seasons with one exception. During a short period end of April 2018, the CRS measured irregularly because of a problem with the connector. However, the CRS then continued measuring without our interference. In summer 2018, we changed the connector and measurements have been without gaps since.

To fill the data gaps, we correlated the measurements at Plaine Morte with all IMIS stations, and a selection of stations from the SwissMetNet. For the parameters SD, air pressure and wind speed, we chose the station with the highest correlation (Table 3). We did not fill the gap of wind direction because all correlations were below 0.45 at hourly as well as daily scale. Because SD is an accumulated time series, we correlated the daily change in SD. The mean bias in Table 3 is used to adapt the reference data to the Plaine Morte station. The standard deviation of the mean bias represents the absolute uncertainty of the parameters during the interpolated time period.

4.2 Calculating SWE and the bulk snow density

The CRS records the total number of cosmic ray neutrons integrated over a one hour period. The neutron intensity, measured in counts per hour (cph), is then used to infer SWE.

In a first step, we pre-process obtained neutron counts as follows: To eliminate spurious changes in the count rate, neutron counts are excluded if the hourly count differs more than 20% from an 6-hour moving average. The neutron counts are then corrected by variations in solar activity and more importantly by air pressure. Variations in solar activity are quantified with the aid of a reference station, which is not buried in the snow (Sigouin and Si, 2016; Howat et al., 2018). As a reference station, we use the nearby neutron monitor at Jungfraujoch (JUNG, www.nmdb.eu, see Fig. 1). Air pressure is directly measured in situ. More detailed information on the pre-processing of the raw neutron counts is provided in the appendix.

After these corrections, the hourly neutron counts are smoothed using a 6-hour moving average. We calculate SWE from the relation

$$SWE_i = -\frac{1}{\Lambda} \cdot \ln \frac{N_i}{N_0} \tag{1}$$

where N_0 is the mean count rate at snow free conditions, N_i is the hourly count rate, and the variable Λ is the effective attenuation length given by

$$\Lambda = \frac{1}{\Lambda_{\max}} + \left(\frac{1}{\Lambda_{\min}} - \frac{1}{\Lambda_{\max}} \right) \cdot \left(1 + exp \left(- \frac{\frac{N_i}{N_0} - a_1}{a_2} \right) \right)^{-a_3} \tag{2}$$

The empirical parameters that were provided by the manufacturer are $\Lambda_{\min}$ (14.1 cm) and $\Lambda_{\max}$ (114.4 cm), a_1 (0.3), a_2 (0.1) and a_3 (1.1). Note that the parameters Λ_{min} and Λ_{max} are respectively the asymptotic values of the effective attenuation lengths for low and high SWE values, and that the parameters a_1, a_2 and a_3 define the curvature of a sigmoidal function. The reference count rate N_0 is determined over the median count rate in July 2017 (4146 cph). Fig. 2a shows the theoretical exponential relation between hourly neutron counts and SWE given by Eq. 1.

https://doi.org/10.5194/tc-2019-106
Preprint. Discussion started: 29 May 2019

Table 3. Time periods of data gaps with reference periods for correlation and correlation coefficients. The mean bias shows the average difference (and its standard deviation) between the reference stations and AWS at Plaine Morte. All stations are shown in Fig. 1

Parameter	Data gap	Reference station Name, Network Coordinates	Correlation periods	Correlation mean bias
snow depth	20 Jan 2018 to 4 May 2018	Gandegg/ Laucherenalp SLFGA2, IMIS 7°46'E, 46°26'N, 2717 masl	4 Nov 2016 to 13 Jul 2017 27 Oct 2017 to 19 Jan 2018 4 May 2018 to 26 Jul 2018	0.86 (daily) 0.1±6.0 cm
air pressure	22 Jan 2018 to 10 Mar 2018	Les Diablerets DIA, SwissMetNet 7°12'E, 46°20'N, 2964 masl	1 Nov 2016 to 22 Jan 2018 10 Mar 2018 to 1 Mar 2018	0.996 (hourly) -23.96±0.6 hPa
wind speed	22 Jan 2018 to 17 Apr 2018	Guttannen/ Homad SLFGU2, IMIS 8°17'E, 46°41'N, 2110 masl	1 Jan 2018 to 22 Jan 2018 17 Apr 2018 to 30 Sep 2018	0.87 (daily) 0.1±1.0 m s^{-1}
temperature	10 Mar 2018 to 17 Apr 2018	Les Diablerets SLFDIA, IMIS 7°15'E, 46°19'N, 2575 masl	1 Jan 2018 to 10 Mar 2018 17 Apr 2018 to 30 Sep 2018	0.96 (hourly) 1.8±2.4 °C
relative humidity	10 Mar 2018 to 17 Apr 2018	Les Diablerets SLFDIA, IMIS 7°15'E, 46°19'N, 2575 masl	1 Jan 2018 to 10 Mar 2018 17 Apr 2018 to 30 Sep 2018	0.78 (daily) -7.8±8.5 %

From the hourly SWE values, we calculate the daily means (SWE_{crs}). The bulk snow density ($\rho_{crs,sr}$, in kg m^{-3}) is then derived from daily SWE (SWE_{crs}, in kg m^{-2}) and daily SD measurements (SD_{sr}, in m) according to

$$\rho_{crs,sr} = \frac{SWE_{crs}}{SD_{sr}} \tag{3}$$

The temporal resolution of one day allows the determination of daily changes in SD, SWE and the bulk snow density. These daily changes are calculated as the difference between two consecutive days. To assure the exclusion of errors, the daily rates have to be larger than the uncertainty estimates (see below).

https://doi.org/10.5194/tc-2019-106
Preprint. Discussion started: 29 May 2019

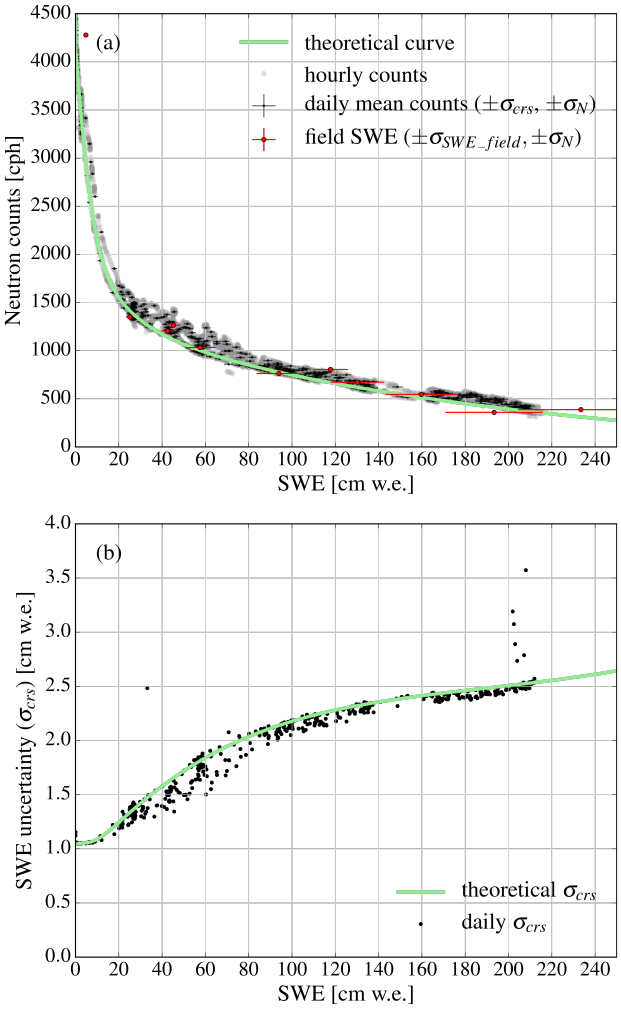

Figure 2. (a) Hourly neutron counts (corrected and smoothed) with calculated SWE amounts (grey dots). Black dots show the average daily neutron counts with average daily SWE amounts. Red crosses show field measurements of SWE and their corresponding daily neutron counts. The error bars refer to the uncertainties. The green line shows the theoretical SWE amounts with the applied N_0. (b) Daily uncertainty of SWE (σ_{crs}) in relation to the daily SWE amounts. The green line represents the theoretical increase in uncertainty with SWE.

4.3 Estimating the uncertainty of automatically derived SWE, SD and snow density

In general, we distinguish between the observed standard deviation of all observed hourly values during one day (s) and the theoretical measurement uncertainty in those daily values (σ). The daily standard deviations of SWE ($s_{\mathrm{SWE\_crs}}$) and SD ($s_{\mathrm{SD\_sr}}$) are derived assuming a gaussian distribution. For the standard deviation of the bulk density ($s_{\rho(\mathrm{crs\_sr})}$), we apply

https://doi.org/10.5194/tc-2019-106
Preprint. Discussion started: 29 May 2019

gaussian error propagation to Eq. 3 to yield

$$s_{\rho(\mathrm{crs\_sr})} = \sqrt{\left(\frac{s_{\mathrm{SWE\_crs}}}{SWE_{crs}}\right)^2 + \left(\frac{s_{\mathrm{SD\_sr}}}{SD_{\mathrm{sr}}}\right)^2} \tag{4}$$

The calculation of the measurement uncertainties of SD (σ_{sr}), SWE (σ_{crs}) and the bulk density (σ_ρ) is described in the following paragraphs. The main source of uncertainty in the SWE estimates (σ_{crs}) is the neutron count uncertainty. This uncertainty is given by

$$\sigma_{N_i} = \sqrt{N_i} \tag{5}$$

and is valid for all temporal resolutions (i). Applying the general error propagation formula on Eq. 1, we derive

$$\sigma_{\mathrm{crs}} = \left(\frac{\partial SWE_{crs}}{\partial N}\right) \cdot \sigma_{\mathrm{N}} + \sigma_{\mathrm{const}} \tag{6}$$

Because the fluctuations of SWE estimates in snow free conditions are $\pm$0.5 cm around 0 cm of snow, we add an additional constant uncertainty of $\pm$1 cm (σ_{const}).

In this study, the calculation of the theoretical uncertainty of the SWE observations is done at the daily resolution. Fig. 2a shows the uncertainty of the daily neutron counts and daily SWE values. Fig. 2b shows the theoretical uncertainty and the daily observed uncertainties, which are lower than in theory. The outliers at round 200 cm SWE result from a short measurements gap end of April 2018. During this gap, some hourly values were missing resulting in an overall lower daily neutron count and a consequently higher uncertainty. We also note that the relative error in SWE slowly decreases with higher SWE amounts. For instance, it is 2% at 100 cm, but 1.3% at 200 cm of SWE.

The uncertainty of daily SD observations varies with the depth of the snowpack. According to the installation manual, the accuracy lies between $\pm$1 cm and 0.4% of the distance from sensor to ground (Campbell Scientific, 2016). Since the sensor is mounted at 4.75 m, the maximum uncertainty equals 1.9 cm under snow free conditions. In addition to the given uncertainty, we add a further systematic measurement uncertainty on SD's less than 30 cm. This uncertainty is caused by the footprint of the sonic ranging sensor which is large enough to include parts of the mast's foundations. The mast's foundation consists of three wooden beams with a height of 20 cm each. They stabilize the mast on the glacier ice, especially during the ice melt season. To keep the wooden beams in place, they are anchored with tubes drilled into the ice. These tubes also exceed the 20 cm height of the wooden beams and add an additional error. We estimate this additional uncertainty to be 30% with SD below 30 cm, 50% with SD below 25 cm, 80% with SD below 15 cm and 100% with SD below 10 cm. Moreover, the SD measurements from 20 January 2018 to 4 May 2018 which have been taken from another station at high-elevation carry an additional uncertainty of 6 cm (see Table 3).

Using the uncertainties of SD and SWE, we derive the uncertainty of the daily bulk density (σ_ρ) as

$$\sigma_{\rho(\mathrm{crs,sr})} = \sqrt{\left(\frac{\sigma_{\mathrm{crs}}}{SWE_{\mathrm{crs}}}\right)^2 + \left(\frac{\sigma_{\mathrm{sr}}}{SD_{\mathrm{sr}}}\right)^2} \tag{7}$$

https://doi.org/10.5194/tc-2019-106
Preprint. Discussion started: 29 May 2019

4.4 Estimating the uncertainty of field data

Field measurements carry uncertainties, which may have different sources (sampling tube, weight scale, sampling technique, etc.). Only few studies discuss the accuracy of SWE observations comprehensively (e.g. Stuefer et al., 2013). Commonly, a relative uncertainty of $\pm 10\%$ is applied (e.g. Schattan et al., 2017). Thibert et al. (2008), for example, focus on uncertainties for glacier mass balance calculations based on the glaciological method. These random and systematic errors, however, assume underlying firn with unknown water content and are not intended for snow accumulation. For our study, we have chosen to calculate an uncertainty based on the gaussian error propagation (see Papula, 2010). Next to the human-induced errors, which cannot be quantified in the scope of this study, we identify two major sources of sampling errors. These are related to the weighed mass and the snow volume within the tube.

We sample an entire column of the snowpack, from the surface to the snow-glacier interface. These samples are taken either within a snow pit, or by extracting a snow core. In both approaches, we use a sampling tube. In deeper snowpacks, the whole column cannot be sampled in one measurement step. Thus, we take several samples with a certain length (l_s) from snow to glacier surface. For each of these samples, the density (ρ_s) is calculated by applying Eq. 8). The variable m_s represents the mass of the snow weighed in situ with a scale, while r_tube represents the radius of the sampling tube.

$$\rho_\mathrm{s} = \frac{m_\mathrm{s}}{\pi \cdot r_\mathrm{tube}^2 \cdot l_\mathrm{s}} \tag{8}$$

The sources of the sample uncertainty in density (σ_{ρ_s}) arise from the uncertainties in snow-mass weighing (Σm_s), the uncertainties of the sampled volume given by the radius (Σr_tube) and the uncertainties of the sampled length (Σl_s) in the snowpack. The uncertainty of the mass is thus composed of two individual sources; the scale for weighing the sample (Σm_scale), and the extracted snow volume (Σm_mass). These two uncertainties are added to Σm_s following Gaussian error propagation. Because the surface area of the extracted snow core does not always match the tube's surface area, we define an uncertainty range for the radius. The relative uncertainty of each sample (σ_{ρ_s}) is then derived from

$$\sigma_{\rho\_\mathrm{s}} = \frac{\Sigma\rho_s}{\rho_s} = \sqrt{\left(\frac{\Sigma m_\mathrm{s}}{m_\mathrm{s}}\right)^2 + \left(2 \cdot \frac{\Sigma r_\mathrm{tube}}{r_\mathrm{tube}}\right)^2 + \left(\frac{\Sigma l_\mathrm{s}}{l_\mathrm{s}}\right)^2} \tag{9}$$

Given the density for each sample at different depths within the snowpack, we calculate the bulk density (ρ_field). To this end, we need to divide the snowpack into layers of variable lengths. Because of this variation, we determine a multiplicative weight p_l for each layer as

$$p_\mathrm{l} = \frac{l_\mathrm{l}}{SD_\mathrm{field}} \tag{10}$$

This weight corresponds to the relative contribution of l_l to the total depth of the snowpack (SD_field) which is measured independently.

The samples may overlap depending on the tube and the extraction method used. If there is no overlap, the length of the sample l_s is equal to the thickness of the layer l_l, and the number of samples is equal to the number of layers (n_l). Simultaneously, the sample density ($\rho_\mathrm{s} \pm \Sigma\rho_\mathrm{s}$) corresponds to the layer density ($\rho_\mathrm{l} \pm \Sigma\rho_\mathrm{l}$). If the samples overlap, ρ_l corresponds

https://doi.org/10.5194/tc-2019-106
Preprint. Discussion started: 29 May 2019

to the mean density and propagated uncertainty of the overlapping samples. In that case, the number of layers is greater than the number of samples. With

$$\rho_{\text{field}} = \frac{1}{n_{\text{l}}} \cdot \sum_{i=1}^{n_{\text{l}}} p_{\text{l},i} \cdot \rho_{\text{l},i} \tag{11}$$

and

$$\sigma_{\rho\_\text{field}} = \frac{\Sigma\rho_{\text{field}}}{\rho_{\text{field}}} = \frac{\sqrt{\sum_{i=1}^{n_{\text{l}}} p_{\text{l},i} \cdot (\Sigma\rho_{\text{l},i})^2}}{\rho_{\text{field}}} \tag{12}$$

we obtain the bulk density (ρ_{field}) and its relative uncertainty ($\sigma_{\rho\_\text{field}}$).

Knowing the bulk density and the depth of the snowpack (SD_{field}), we calculate the total amount of SWE (SWE_{field}) with

$$SWE_{\text{field}} = \rho_{\text{field}} \cdot SD_{\text{field}} \tag{13}$$

With error propagation by Gauss, we derive the relative uncertainty of SWE as

$$\sigma_{\text{SWE\_field}} = \frac{\Sigma SWE_{\text{field}}}{SWE_{\text{field}}} = \sqrt{\left(\frac{\Sigma\rho_{\text{field}}}{\rho_{\text{field}}}\right)^2 + \left(\frac{\Sigma SD_{\text{field}}}{SD_{\text{field}}}\right)^2} \tag{14}$$

The absolute uncertainty of SD_{field} (ΣSD_{field}) is estimated independently of the sample measurements. The absolute uncertainty of the bulk density ($\Sigma\rho_{\text{field}}$) is given in Eq. 12.

For each field campaign we define the discussed uncertainty depending on the sampling tube, the scale, and whether we sampled within a snow pit or extracted a snow core. Thereby, we use four different tubes with a radius of 4.00±0.10 cm, 4.15±0.15 cm, 4.50±0.10 cm and 4.75±0.10 cm and a length of 117.0 cm, 107.0 cm, 55.7 cm and 56.0 cm, respectively. Additionally, we have three scales with a maximum weighing capacity of 2±0.02 kg, 5±0.05 kg and 12±0.10 kg. The uncertainty in the weighed mass ranges from 0.05 kg to 0.15 kg depending on the snow depth and the tube length. Sampling lengths are attributed with an uncertainty between 0.5 cm and 1.0 cm. During a field campaign, we usually sample more than one column. In those cases we take an average of all snow parameters, and we average all σ to account for the mean uncertainties. We quantify the variability within several snow columns with their standard deviation (s) which is smaller than the mean uncertainty. An extensive table on all assumed uncertainties, the number of samples per snow pit is provided in the supplement.

4.5 Pre-processing precipitation data

Precipitation data from nearby stations at lower elevations are compared to snow accumulation observed by the CRS. The precipitation data have an hourly resolution measured from HH:01 to (HH+1):00. For comparison, we sum the hourly values to daily precipitation amounts. The time series of the precipitation sums begins at the same day as the snow accumulation observations. That implies adding a constant value to the cumulative precipitation series in the second winter because the snowpack was already advanced when observations began. The end of the time series is set at the end of May for each year. At this point in time, the peak of SWE had already passed in both winters.

https://doi.org/10.5194/tc-2019-106
Preprint. Discussion started: 29 May 2019

To find a suitable scaling factor, all daily precipitation sums are multiplied by the same scaling factor and compared to the snow accumulation. In the second winter season, we also add a constant factor so that snow accumulation and precipitation begin with the same amounts. The comparison is analyzed by the mean absolute error (MAE) and its standard deviation over the whole time series at the daily resolution. For each station, we have 392 days available for comparison.

In a more elaborate approach, hourly temperature data from the station at Plaine Morte are included. Therefore, we categorize days with only liquid, only solid, and a mixture between liquid and solid precipitation. For the distinction, we introduce temperature thresholds based on previous studies. The study by Sims and Liu (2015), for instance, shows that 90% of precipitation events were solid precipitation for near-surface temperatures below 0°C for land surface observations. For temperatures above 3°, more than 85% of all precipitation events were liquid. Therefore, we consider all precipitation as liquid if temperatures are above 3°C during at least six hours. If temperatures range between 0°C and 3°C during at least six hours, we classify it as mixed-phase precipitation. Thereby, all days with such a classification are used to determine the optimal scaling factor. If the two previous criteria do not apply or the daily maximum temperature does not exceed 0°C, it is solid precipitation. For these classified days, we evaluate the optimal scaling factor applying the same procedure as described above.

5 Results

5.1 Measured snow depth, SWE and snow density

With the CRS installed on Plaine Morte, SWE was measured during two subsequent winter seasons (2016/17 and 2017/18). These two winters were markedly different, with the second winter experiencing particularly heavy snowfall. During winter 2016/17, a maximum SD of 324 cm was reached on 2 May 2017 and a maximum SWE (137 cm w.e.) on 18 May 2017. With these observations, the first winter season lies in the range of average mean specific winter mass balances between 2009 to 2017 (GLAMOS, 1881-2018). During the following winter 2017/18, a maximum of 520 cm of SD (1 April 2018), and a maximum SWE of 212 cm w.e. (24 May 2018) were observed, which corresponds to about 1.5 times of SWE than in the previous year.

Fig. 3a and c show snow accumulation and ablation over the two winter seasons. In both winters, the first snowfall around mid-October led to SDs of about 20 cm. By mid-November, SD exceeded one meter with approximately 30 cm w.e. in both winters. In winter 2016/17, the SD remained almost constant until the beginning of January 2017. In the subsequent winter, SD significantly increased from November 2017 to January 2018. By that time, it had already surpassed the maximum in SD of the previous winter.

From January 2017 to Mai 2017, SD increased almost continuously with a period of accumulation followed by a period of densification. The time lag between the maximum of SD and the maximum of SWE is 16 days. During this time span, SWE remained almost constant and only increased little. By the beginning of July 2017, the snow had melted. In winter 2017/18, SWE increased more continuously between end of January and beginning of June. In this winter, the maxima in SD and SWE are almost two months apart. Already in April 2018, SD started decreasing while SWE remained constant. During that time, only few events led to small increases in SD. From end of Mai 2018 onwards, SWE decreased rapidly. By the end of July, the snow had disappeared.

https://doi.org/10.5194/tc-2019-106
Preprint. Discussion started: 29 May 2019

The Cryosphere
Discussions
Open Access
EGU

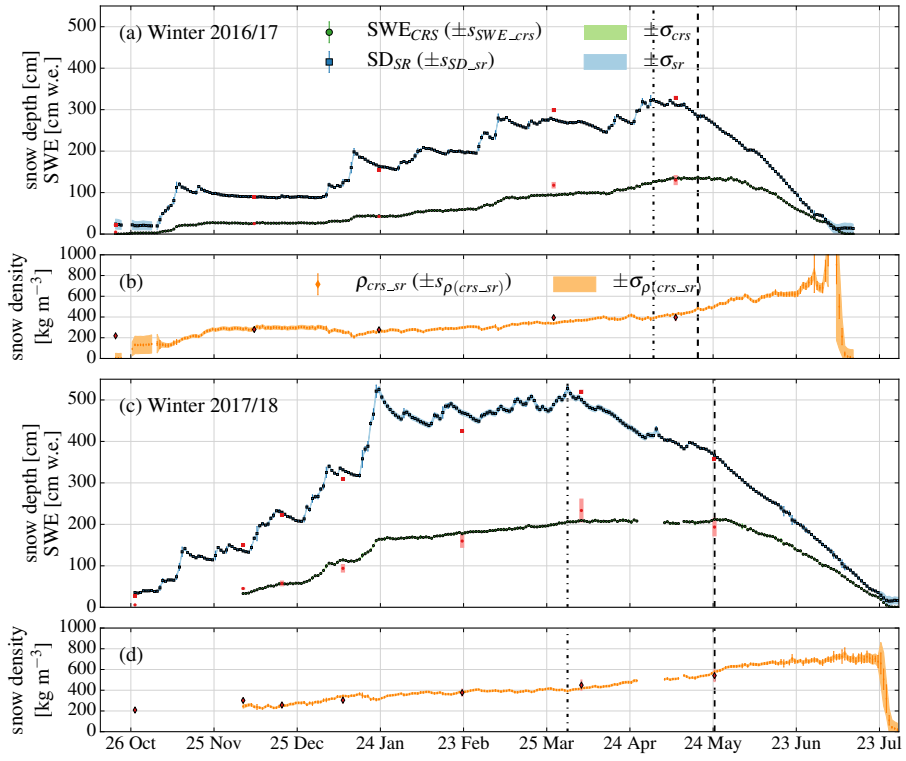

Figure 3. Blue squares show daily mean snow depths (SD), green dots daily mean SWE values during winter 2016/17 (a) and winter 2017/18 (c). The shading corresponds to the theoretical uncertainty, while bars represent the daily standard deviation. Red squares and dots represent manual measurements of SD and SWE, respectively. Salmon bars show the uncertainty of the field measurements. (b) and (d) show daily mean snow density with its uncertainty (orange shading). Red diamonds show the manual field measurements with their uncertainty (salmon bars).

With the daily observations of SWE and SD, we calculate the daily bulk snow density. Fig. 3b and d show its evolution over time. In the beginning of winter 2016/17, for instance, snow density increases after a short decrease. This short increase corresponds to the snowfall observed in Fig. 3a. In general, densification slowly progresses with short intervals of decreasing densities caused by snowfall. Between the maximum SD and the maximum SWE, density increases almost linearly in both winters. After reaching the maxima of SWE, snow densities are above 500 kg m^{-3}. Shortly before the snowpack disappears completely, densities decrease but carry larger uncertainties.

Fig. 4 shows daily SWE in relation to daily SD over the winter season. During the accumulation period, daily densities vary between 200 kgm^{-3} and 400 kgm^{-3}. Often, an increase in SD is followed by a period where SWE remains constant and SD decreases. This marks periods of snow densification. In general, both winters follow a similar pattern in the evolution of density. At the maximum of SD, the daily density is 390 kg m^{-3} for winter 2016/17 (2 May 2017) and 392 kg m^{-3} for winter 2017/18 (1 April 2018). After these peaks, the snowpack begins to densify continuously. During this period of densification,

https://doi.org/10.5194/tc-2019-106
Preprint. Discussion started: 29 May 2019

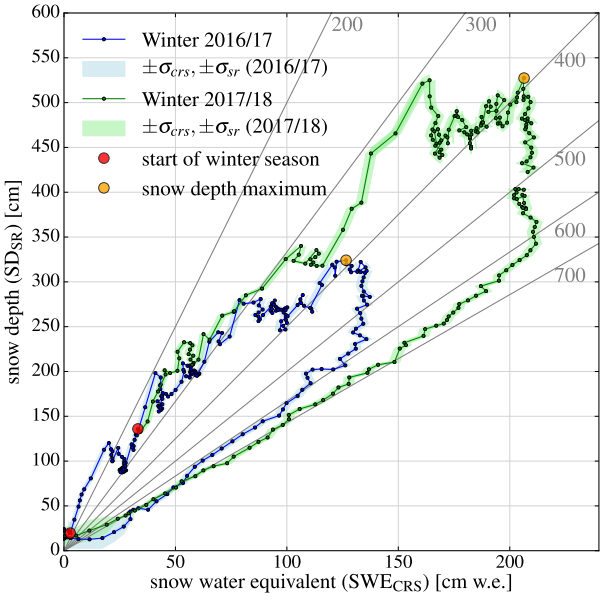

Figure 4. Daily mean SWE and daily mean SD. Grey lines show the densities in kg m^{-3}. The beginning of each winter season is marked by the red dot, yellow dots indicate the maximum of SD.

SWE remains almost constant while SD decreases by about 1 m (2016/17) and 1.5 m (2017/18). Only then does the SWE begin to decrease simultaneously with SD, following the density lines between 600 kg m^{-3} and 700 kg m^{-3}.

For the evaluation of the CRS, we obtained field data during 11 campaigns over the two winter seasons. Fig. 5 shows the autonomous data of SWE (Fig. 5a), SD (Fig. 5b) and snow density (Fig. 5c) compared to the data from the field surveys. On average, the CRS overestimates SWE by +2%±12%. The SD measurements agree within a standard deviation of ±6%, and ±7% when also considering the interpolated data during the measurement gap of SD. The snow density data agree on average with a standard deviation of ±8% (Fig. 5d). Furthermore, the uncertainties of the field data are always higher than the estimated uncertainties of the automatic measurements. This is due to the higher precision of the automatic measurements, the undisturbed snowpack, and the exclusion of potential human-induced errors. The correlation coefficients (r^2) of all considered snowpack parameters are higher than 0.90 (Fig. 5).

5.2 Daily variations of SWE and SD

From the continuous data of SWE and SD, we can evaluate the daily variations. Fig. 6a shows this day-to-day variations of SWE and SD. With this information, we can distinguish days dominated by general processes affecting the snowpack such as accumulation, densification and ablation. To this end, we define a criterium for SWE and SD considering the uncertainties of the measurements. The uncertainties are especially important for the SWE measurements as we want to distinguish between noise and signal. Table 4 gives an overview of all criteria and the number of days when these are satisfied. A day dominated

https://doi.org/10.5194/tc-2019-106
Preprint. Discussion started: 29 May 2019

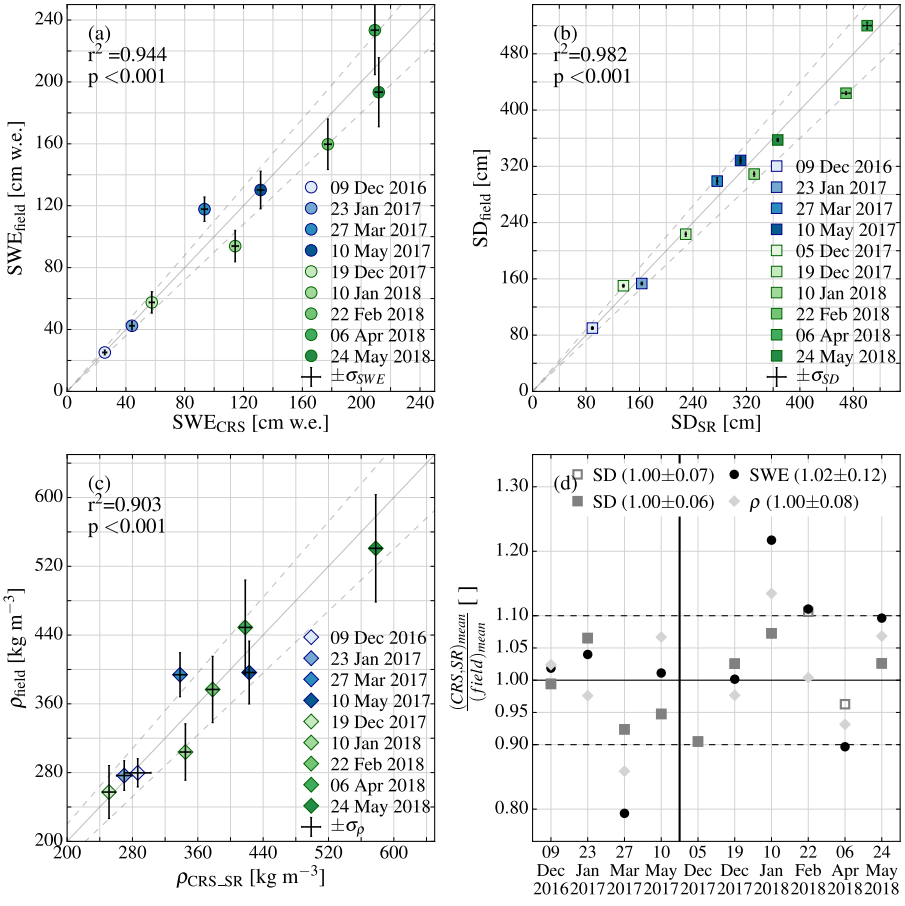

Figure 5. Scatter plots of the field data compared to the automatic measurements of SWE (a), SD (b) and bulk snow density (c). The dashed grey lines show the range within ±10%. (d) shows the ratio between field and automatic measurements for SD, SWE and snow density (ρ). The unfilled grey squares represent the data interpolated from another station.

by accumulation has to have a change in SD greater σ_{sr}, while the change in SWE has to be greater than 0 cm. To ensure more confidence (accumulation with high confidence), the SWE changes have to exceed σ_{crs} (Table 4). The same applies for ablation with the difference that the daily change has to be more negative than the uncertainty values. For densification, we require a significant decrease in SD while SWE remains constant or increases. For the latter case, we extract the days where densification and accumulation occur on the same day. Fig. 6b shows that the winter is mainly dominated by accumulation and densification. Some days with ablation occur at the beginning of March 2017. On these days, we note higher wind gusts and subzero temperatures (Fig. 6c,d). Hence, ablation is likely caused by snow drift rather than melt. Ablation through snow melt sets in as soon as daily air temperatures are above 0 °C.

https://doi.org/10.5194/tc-2019-106
Preprint. Discussion started: 29 May 2019

Table 4. Definition of the process-dominated days with the color displayed in Fig. 6, the criteria and the number of days.

Process	color	snow depth	SWE	days (2016-2018)	days (2016/17)	days (2017/18)
all	-	-	-	484 (100%)	260 (100%)	224 (100%)
accumulation	lightblue	$> \sigma_{sr}$	> 0 cm	112 (23%)	58 (22%)	54 (24%)
ablation	red	$< -\sigma_{sr}$	$< -\sigma_{crs}$	73 (15%)	28 (11%)	45 (20%)
densification	green	$< -\sigma_{sr}$	≥ 0 cm	210 (43%)	101 (39%)	109 (49%)
not classified	white	-	-	89 (18%)	73 (28%)	16 (7%)
subgroups						
accumulation (high confidence)	blue	$> \sigma_{sr}$	$> \sigma_{crs}$	61	32	29
densification with accumulation	lightgreen	$\leq 0\ cm$	$> \sigma_{crs}$	28	14	14

The mean daily meteorological conditions can be summarized for the categorized days (Fig. 7, Tab. 4). Days with accumulation are characterized by high relative humidity (Fig. 7a), significantly lower temperatures (Fig. 7b) and an average decrease in mean density (Fig. 7c). Wind speeds are higher and originate mainly from south over west to north. Days dominated by ablation are characterized by average daily relative humidity (Fig. 7a), significantly higher temperatures (Fig. 7b) and lower wind speeds (Fig. 7d). During the ablation days, we find no significant change in density. Days with densification have lower daily relative humidities than days with ablation. The median values of daily mean temperatures and daily mean wind speeds are similar to the ones in the reference periods. During days with densification, the wind direction is mostly south-east.

All these findings align with our general expectations that accumulation occurs with lower temperatures, high relative humidity, and stronger winds. Ablation through melt is mainly characterized by higher temperatures, lower relative humidity and lower wind speeds. Of all densification days, 11% show a simultaneous increase in SWE ("densification with accumulation", Table 4). When both processes occur at the same day, it suggests either simultaneous compaction of snowfall, accumulation by snow drift, or infiltration of liquid precipitation. About one third of these days have daily mean temperatures above 0 °C which suggest infiltration. Another third of these days have daily mean wind speeds above 4 m s^{-1}, which suggests snow drift. The last third have negative mean temperatures and wind speeds below 4 ms^{-1}.

5.3 Comparison of snow accumulation to precipitation observations

The daily observations of SWE on Plaine Morte allow a comparison to daily precipitation sums from nearby weather stations at lower elevations and gridded precipitation (RhiresD). In the following, we refer to the autonomous CRS measurements as snow accumulation, and cumulative precipitation from other sources as precipitation sums.

Fig . 8 shows the cumulative precipitation of three nearby stations at lower elevations, including Adelboden (1322 masl) and Montana (1427 masl, Table 2). In addition, cumulative precipitation from three grid cells of RhiresD are included (grid cells 1-3). As to be expected, precipitation sums are significantly lower than snow accumulation on the glacier. This is mainly due to orographic effects but could also be caused by snow drift, or undercatch of the rain gauge. In general, the timing of increases

https://doi.org/10.5194/tc-2019-106
Preprint. Discussion started: 29 May 2019

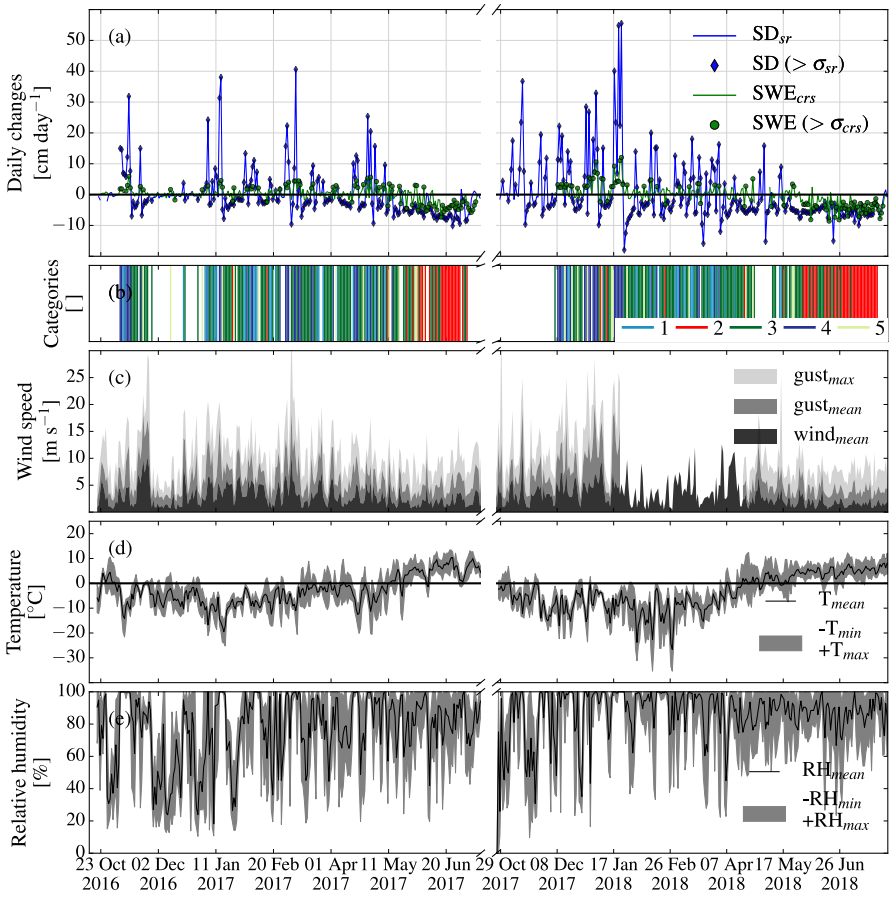

Figure 6. (a) Daily rates of SD (blue) and SWE (green). (b) Categorization of process-dominated days with 1 as accumulation, 2 as ablation, 3 as densification, 4 as accumulation with high confidence, and 5 as densification with accumulation (see Table 4). (c) Daily mean wind speeds (black shading), mean wind gusts (grey shading) and daily maximum wind gust (light grey shading). (d) Daily mean temperature (black line) with daily maximum and minimum temperature (grey shading). (e) Daily mean relative humidity (black line) with daily minimum and maximum relative humidity (grey shading).

in snow accumulation corresponds well with increases in the precipitation observations. Still, there are some exceptions as, for instance, in mid of December 2016 (Fig. 8). In addition, during some time periods accumulation increases more strongly than precipitation (e.g. mid-April 2017). During most of such time periods, daily mean wind speeds remain below 6 m s^{-1}. Mean daily wind gusts are mostly below 10 m s^{-1} (Fig. 6c). Nonetheless, snow drift cannot be excluded to locally increase snow accumulation.

In the second winter, it is evident that the sums during single precipitation events are lower than for snow accumulation. This is the case until mid of January 2018. During most of December 2017, mean daily wind speeds are above 5 m s^{-1} (Fig. 6c). Thus, snow drift may cause these discrepancies. Our analysis of days dominated by accumulation (Fig. 7) shows that wind

https://doi.org/10.5194/tc-2019-106
Preprint. Discussion started: 29 May 2019

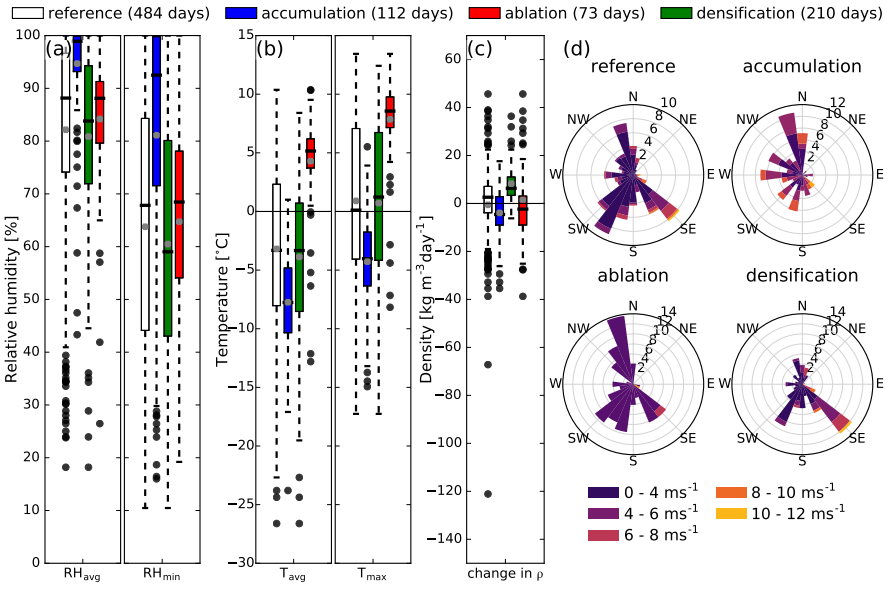

Figure 7. Summary of daily values of the daily mean and minimum relative humidity (a), daily average and maximum temperature (b) and the change in mean bulk snow density (c). (d) shows mean daily wind speeds with wind direction. The numbers in the wind roses correspond to the percentage of days within that selection. The reference includes all days with valid data.

Table 5. Scaling factors resulting in a minimal MAE. Two different approaches are presented; one factor applied and three factors applied distinguishing between the precipitation regimes (solid, mixed and liquid).

	one factor		three factors			
	all [ ]	MAE [cm]	solid [ ]	mixed [ ]	liquid [ ]	MAE [cm]
Adelboden	2.8	7.8±5.7	2.9	1.8	0.2	4.1±3.8
Montana	3.3	7.6±4.3	3.4	3.4	0.2	5.6±3.6
Tsanfleuron	1.8	7.1±3.6	1.8	2.0	0.2	5.4±2.5
grid cell 1	1.5	7.3±4.4	1.5	1.2	0.1	4.7±4.1
grid cell 2	1.4	7.4±6.0	1.5	1.2	0.1	4.0±2.8
grid cell 3	1.6	7.9±7.1	1.7	1.3	0.1	4.6±4.2

speeds are mostly higher 8 $\mathrm{m\,s^{-1}}$ and that the direction does not vary strongly during such days. This suggests an almost constant influence of snow drift.

Using the continuous time series of snow accumulation on Plaine Morte, we determine the precipitation scaling factor for each weather station and grid cell which leads to a minimal MAE for the reproduced accumulation on the glacier over the two

https://doi.org/10.5194/tc-2019-106
Preprint. Discussion started: 29 May 2019

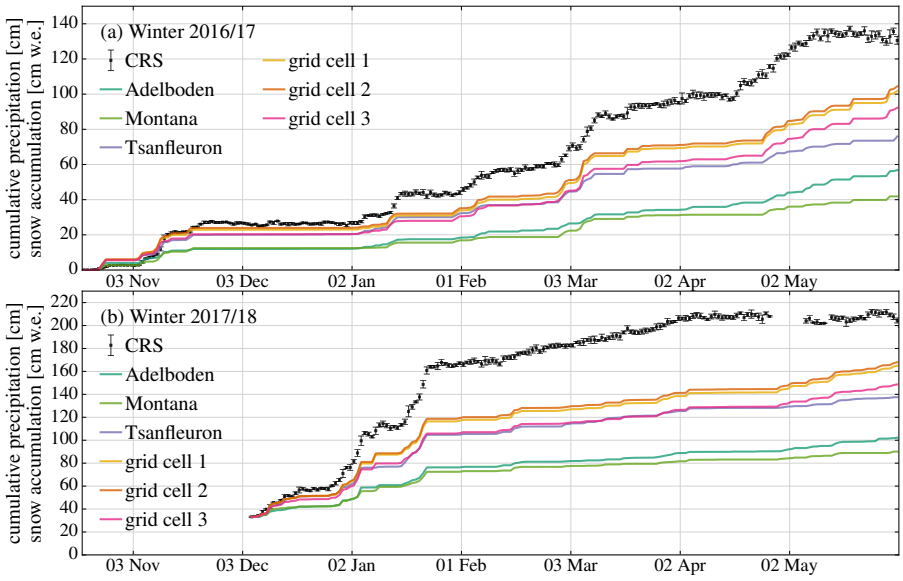

Figure 8. Cumulative precipitation and snow accumulation of (a) winter 2016/17 and (b) winter 2017/18. Black squares show the daily measured means with daily standard deviations of the SWE measurements. Cumulative precipitation is corrected with a constant bias to fit the beginning of measurements.

winter seasons. The gridded precipitation has similar scaling factors (Table 5). The precipitation measured at Tsanfleuron has a scaling factor in a similar range as for the grid cells. The two stations which are located at elevations around 1400 m lower than the measurements at Plaine Morte, have scaling factors of 2.8 (Adelboden) and 3.3 (Montana). Applying the given scaling factors, we can reproduce snow accumulation with a MAE of below 8 cm w.e. The best performance is found for the station at Tsanfleuron with a MAE of 7.1±3.6 cm. We find that accumulation events in October/ November 2016 are not well reproduced by the scaled weather station precipitations; accumulation is overestimated by at least 5 cm (Fig. 9a,b). The same observation has been made for May 2017. In these months, hourly temperatures at Plaine Morte can reach values higher than 0°C (Fig. 9e). It is thus likely that precipitation falls in its liquid rather than its solid form. Nonetheless, it may still contribute to the SWE by refreezing. However, this effect is only relevant within an isothermal snowpack.

With the applied distinction of the precipitation phase, we find 68 days (17%) with liquid precipitation, 288 days (72%) with solid precipitation, and 46 days (11%) when precipitation is most likely a mixture between solid and liquid precipitation. For each of these precipitation regimes, we derive an optimal scaling factor for each station (Table 5) and calculate snow accumulation (Fig 9c). The scaling factor for solid precipitation remains similar to the ones for the whole time series (Fig. 9a). Mixed-phase precipitation is scaled by slightly lower factors. Liquid precipitation, however, shows factors smaller one (Table 5). With these scaling factors we can reduce the MAE of precipitation to snow accumulation to below 6 cm w.e. With the newly scaled time series (Fig. 9c), the reproduction of snow accumulation through precipitation observations is improved. It especially affects the beginning of winter 2016/17 and the end of May 2017/18. After the accumulation-phase correction, grid

https://doi.org/10.5194/tc-2019-106
Preprint. Discussion started: 29 May 2019

The Cryosphere
Discussions
Open Access
EGU

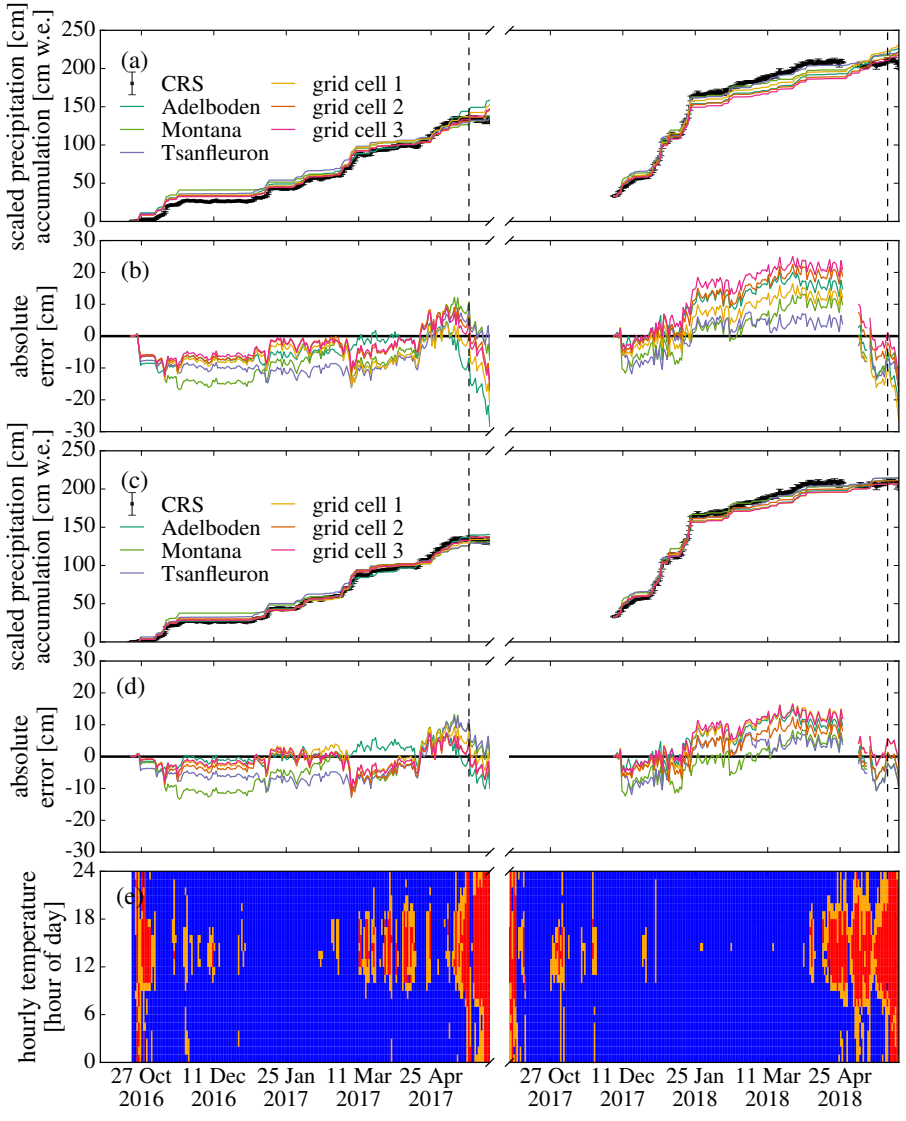

Figure 9. (a) Time series of the scaled cumulative precipitation with one scaling factor per station. (b) Absolute difference between the scaled precipitation and observed accumulation. (c) Time series of the temperature-scaled cumulative precipitation. (d) is the same as (b) for the temperature-scaled precipitation. The scaling factors are provided in Table 5. (e) Hourly temperature at Plaine Morte with temperatures above 3°C (red), between 0°C and 3°C (orange), and below 0°C (blue).

cell 2 has the lowest MAE with 4.0±2.8 cm. This grid cell is directly located above the station at Plaine Morte. The weather station in the south of the glacier, Montana, has the lowest performance with a MAE of 5.6±3.6 cm.

https://doi.org/10.5194/tc-2019-106
Preprint. Discussion started: 29 May 2019

6 Discussion

6.1 Instrument performance and limitations

In this study, we used a CRS in combination with a sonic ranging device to measure and compare snow accumulation over two winter seasons. The evaluation with manual field measurements showed an average overestimation of +2% of SWE values by the CRS. We found that the manual field measurements carry a higher uncertainty than the autonomous CRS measurements of SWE. By taking this uncertainty into consideration, we suggest that SWE observed by the CRS lies within the uncertainty range of the manual measurements (Fig. 5a). However, during two field campaigns (27 March 2017 and 10 January 2018) the difference between automated and manual measurements of SWE exceeds 20%. The SD measurements are also under- and overestimated by more than 5%, resulting in a difference larger 10% of the bulk snow density. Possible explanations can be attributed either to the field observations or to the CRS measurements. There might have been errors introduced when obtaining the field data. Another possibility is a potential problem in the calculation of SWE from neutron counts at SWE values between 90 and 120 cm. Furthermore, a spatial bias may be introduced: snow pits have never been dug directly above the CRS because of their destructive nature. In fact, it is the most likely explanation for discrepancies in seven of nine field surveys.

The SWE calculations from neutron counts are not too sensitive to the initial count rate N_0 when SWE is greater than approximately 40 cm. For SWE values above 40 cm, it hardly influences resulting SWE values due to the exponential nature of the conversion equation (Eq. 1). Moreover, the calculated SWE fluctuates between –0.5 cm and 0.5 cm during snow-free conditions. We take this into account by adding an additional uncertainty in Eq. 6. In general, the uncertainty estimate presented here is rather generous. The straightforward and robust data processing is one of the advantages of the CRS.

Directly comparable to our study is the study by Howat et al. (2018), where they deployed a CRS on the Greenland ice sheet. With the variability of SWE estimations, they define a precision of 0.7%. This precision is significantly lower than our uncertainty range. Generally higher neutron counts and lower SWE values place Howat et al. (2018) on a stepper part of the calibration curve which results in more precise results. The level of noise is also lower at higher neutron counts. In our study, we define the uncertainty range such that it includes the noisiness of the neutron counts. In addition, we integrate the temporal resolution to daily values because of the noise. Overall, the noise levels can be reduced by either integrating the neutron counts over a longer time period or by adding more neutron detectors. In the latter case, however, it becomes quite costly.

In general, one could argue that a snow scale or snow pillow would have been more suitable for such an analysis, especially given the higher temporal resolution during the accumulation phase. However, such devices are not well suited for this site because of the surface roughness of the glacier, the lack of a large flat surface and the changing surface by ice melt. In addition, ice bridging would have been problematic. For sub-snow GPS, one problem might be the glacier movements or the surface melt. In addition, data processing is different for dry or wet snow and is therefore more complicated.

The snowpack of the presented winters here evolved differently in terms of amounts and accumulation rates. Simultaneously, the evolution of the mean density of the snowpack is very alike between the two winter seasons. The evolution before the onset of melt agrees well with the findings of Mizukami and Perica (2008). However, snow densities become quite high (>600 kg m^{-3}) during the melt season in our study. Saito et al. (2012) present similar graphs as to Fig. 4. Nevertheless, mean

https://doi.org/10.5194/tc-2019-106
Preprint. Discussion started: 29 May 2019

densities after the SD maxima did not exceed 500 kg m^{-3}. Another study conducted in the Austrian Alps by Schattan et al. (2017) also shows lower mean snow densities towards the end of the snowpack. Schattan et al. (2017) argue that the surrounding patchy snow distribution biases the point-scale measurements of SWE. Even though they used an above ground CRS, which provides a larger sampling area, the CRS setup of our study may also be affected by such influences. Many effects may lead to high densities; water-saturated snow, refreezing of liquid water at several layers within the snowpack or accumulation of liquid water around the CRS which eventually refreezes. With the CRS and the sonic ranging sensor, we can only determine a mean snow density. Therefore, not all these effects would be identifiable, and explanations remain speculative. Despite all potential explanation for errors by the CRS, it could also be a problem with the SD measurements rather than the SWE measurements.

In our study setup, several reasons could cause erroneous SD measurements. Firstly, the snow area below the sonic ranging sensor may show a small depression because of wind turbulence caused by the mast. Furthermore, the snow around the metal mast melts faster possibly leading to a depression with a larger radius around the mast. It remains difficult to assess whether the radius of this depression would be within the footprint of the sonic ranging sensor. Nevertheless, these two effects may superimpose. Secondly, we had to free the solar panels by digging a snow pit around the mast in winter 2017/18. This snow pit would have been refilled by wind, but densities are different probably causing accelerated melt rates around the mast. Thirdly, the influences of the mast's foundations, the wooden beams with the metal anchorage, may cause erroneous SD measurements for more shallow snowpacks. This also becomes clear since SD measurements never reach 0 cm (Fig. 3).

6.2 Comparing observed snow accumulation to precipitation observations

We directly compared measured snow accumulation to precipitation sums of nearby stations and grid cells of RhiresD. With this comparison, we aimed at reproducing snow accumulation by using surrounding stations with precipitation measurements. Precipitations sums which are taken from the nearby weather stations are expected to show lower accumulation amounts. Snow drift, orographic effects, different temperature regimes, etc. lead to higher amounts of snow accumulation than precipitation sums. In the case of RhiresD, the spatial resolution of 1×1 km does not suffice for the complex topography. In reality, the measurement site is at a higher elevation than in RhiresD, and may therefore lead to precipitation sums that are too low.

Despite all caveats, we are able to reproduce the evolution of snow accumulation with a MAE below 8 cm w.e and with a standard deviation of below 8 cm w.e. This MAE is in the same range for all compared stations. With the information of temperature at Plaine Morte, we can even improve the scaling of precipitation. For solid precipitation, the factor is almost the same. The main improvement occurs during days where temperatures are above 3 °C during at least six hours. During such days, precipitation adds little to the snowpack. Nonetheless, we would still expect an increase in SWE at deeper snowpacks due to the refreezing process. Several reasons could explain why we do not see this behavior; Firstly, the CRS might not be able to capture water infiltration because of its noise levels from April to Mai, where SWE values are above 100 cm w.e. Infiltrated water of the snowpack may refreeze at a different location due to lateral transport. For instance, a superficial pond of water close to the mast installation was observed in the field campaign of May 2018. Not many devices would be able to capture such a process automatically. Liquid water that penetrates the whole snowpack and refreezes below the sensor is not registered by the sensor. Secondly, some of the precipitation at Adelboden in May 2018, for instance, resulted from thunderstorms. These

https://doi.org/10.5194/tc-2019-106
Preprint. Discussion started: 29 May 2019

amounts have a short, but high peak and may not have occurred in the same intensity on the glacier. Thus, precipitation amounts would be smaller on the glacier. Thirdly, the infiltration of water into the snowpack would warm the top layers of the snowpack by latent heat release of the refreezing water. Consequently, faster melt rates would be favored after the precipitation event. Independently, sublimation could also occur beforehand. With the daily resolution, such processes cannot be identified as we need a sub-daily resolution. But at higher temporal resolutions, noise levels of the CRS would override signals within the deep snowpack. Only considering changes in SD, we see no increases of SD from mid of May to end of May (Fig. 6b). During this period, most precipitation events are classified as either liquid or mixed-phase. From mid of March to mid of April 2017, some accumulation events result in increases of SD below 10 cm. These events do not have a signal in the SWE measurements (Fig. 6a).

Another uncertainty is introduced by the temperature thresholds applied in this approach. Previous studies have shown that the snow-rain threshold varies on a global scale between –0.4°C and 2.4 °C in the Northern Hemisphere (e.g. Jennings et al., 2018). To refine the temperature thresholds, we need a higher temporal resolution of SWE measurements. Even though we have a higher temporal resolution of SD observations, we cannot identify liquid precipitation with it.

7 Conclusions and perspectives

During two winter seasons, we measured snow accumulation and ablation on a Swiss glacier at daily resolution. The installed CRS showed good performance in comparison to in situ observations with an average overestimation of the SWE of 2%±12%. The automatically derived mean densities agreed on average with a standard deviation of ±8%. With the daily mean snow density observations, we could show that the evolution of the bulk snow density was quite similar for two very different winter seasons. We investigated environmental conditions that led to changes in the snowpack at a daily resolution. Days with accumulation, ablation and densification could be attributed to days with specific prevailing meteorological conditions at this site.

The availability of snow accumulation at daily resolution allows the direct comparison of high-elevation accumulation with precipitation of nearby stations at lower elevations. Optimal scaling factors were evaluated for different stations and grid cells of RhiresD. With the scaling factors, the snow accumulation could be reproduced with a MAE below 8 cm. Taking temperature into account, the MAE could be further reduced to below 6 cm. Even though the approach of scaling precipitation to snow accumulation is strongly simplified, it is effective for reproducing the evolution of snow accumulation at a daily resolution.

In summary, we conclude that the CRS is so far the most suitable measurement device for measuring SWE continuously in cryospheric high alpine environments. Despite its limitations through the level of noise, and its high uncertainties in a very deep snowpacks, it is suitable for long-term monitoring of SWE in high-mountain regions as well as polar regions. In such areas, its robustness in harsh environmental conditions, its rare need for maintenance (once it is properly running), its little demands regarding site topography and its straightforward data processing with little sensitivities to input parameters make it an ideal device for continuous SWE measurements. For more shallow snowpacks, the temporal resolution can be increased to a sub-daily scale. Concerning a financial aspect, the sensor itself lies in the cost range of other devices for SWE observations.

https://doi.org/10.5194/tc-2019-106
Preprint. Discussion started: 29 May 2019

For this study, we chose a costly measurement setup. But for long-term monitoring of SWE, such an extensive installation would not be necessary.

Future studies could analyze the spatial footprint of a CRS lying below the snowpack. Furthermore, spatial distribution of continuous SWE measurements would allow further understanding of the spatial variability in snow accumulation, solid precipitation, precipitation phases and its relation to snow accumulation.

Data availability. All observations at the Glacier de la Plaine Morte are available upon request from the first author. In future, it will also be available in an online repository.

Appendix A: Correcting raw neutron counts

The correction of the raw neutron counts (N_{raw}) to account for in situ influences has been presented in previous studies (Zreda et al., 2012; Sigouin and Si, 2016; Andreasen et al., 2017; Howat et al., 2018). In this study, we apply the same equations. The neutron counts of the CRS are corrected with the solar activity (F_{s}) and the in situ air pressure (F_{p}, Eq. A1).

$$N = N_{\mathrm{raw}} \cdot F_{\mathrm{s}} \cdot F_{\mathrm{p}} \tag{A1}$$

The correction factor F_s is determined as

$$F_{\mathrm{s}} = 1 + \beta \cdot (F_{\mathrm{sol}} - 1) \tag{A2}$$

The variable F_{sol} represents the 13-hour centered rolling mean of the neutron counts at Jungfraujoch (JUNG) divided by the hourly neutron count values. The unit less scaling parameter β, provided by the manufacturer, is 0.95 in this study. It has been determined by the location of the mast installation at Plaine Morte (46.4N, 7.5E, 2700 m) relative to the neutron monitor station at Jungfraujoch (Fig. 1). The correction factor for pressure is calculated as

$$F_{\mathrm{p}} = exp\left(\frac{p - p_0}{L}\right) \tag{A3}$$

The attenuation length L is assumed to be 132 hPa. The hourly pressure values are represented by p, and p_0 stands for an arbitrarily chosen pressure reference (739 hPa).

Author contributions. RG prepared the manuscript, performed field work and data analysis with contributions from all co-authors. NS and MH contributed to the design and execution of the study. DD gave essential inputs on how to process the output of the cosmic ray sensor and define its measurement uncertainty.

Competing interests. Authors RG, NS and MH declare that they have no competing interests. Author DD is the owner of Hydroinnova LLC.

https://doi.org/10.5194/tc-2019-106
Preprint. Discussion started: 29 May 2019

Acknowledgements. This study is supported by the Swiss National Science Foundation (SNSF), grant 200021_178963. MeteoSwiss provided the data of all stations besides the one at Plaine Morte. Jungfraujoch neutron monitor data were kindly provided by the Cosmic Ray Group, Physikalisches Institut, University of Bern, Switzerland. We like to thank H. Gubler from ALPUG, W. Jäger from WALJAG and T. Sarbach from Sarbach Mechanik GmbH. They designed the mast, programmed the logger box, and helped with the field installation. Furthermore, we like to acknowledge all the field helpers during the two winter seasons. Without them, this study would not have been possible.

https://doi.org/10.5194/tc-2019-106
Preprint. Discussion started: 29 May 2019

References

Ali, S. A., Aadhar, S., Shah, H. L., and Mishra, V.: Projected Increase in Hydropower Production in India under Climate Change, Scientific Reports, 8, 12 450, 10.1038/s41598-018-30489-4, 2018.

Andreasen, M., Jensen, K. H., Desilets, D., Franz, T. E., Zreda, M., Bogena, H. R., and Looms, M. C.: Status and Perspectives on the Cosmic-Ray Neutron Method for Soil Moisture Estimation and Other Environmental Science Applications, Vadose Zone Journal, 16, 0, https://doi.org/10.2136/vzj2017.04.0086, 2017.

Barnett, T. P., Adam, J. C., and Lettenmaier, D. P.: Potential impacts of a warming climate on water availability in snow-dominated regions, Nature, 438, 303–309, https://doi.org/10.1038/nature04141, 2005.

Campbell Scientific, I.: Instruction Manual SR50A, SR50A-316SS and SR50AH Sonic Ranging Sensors, revision: 10/16 edn., https://s.campbellsci.com/documents/us/manuals/sr50a.pdf, 2016.

Castebrunet, H., Eckert, N., Giraud, G., Durand, Y., and Morin, S.: Projected changes of snow conditions and avalanche activity in a warming climate: The French Alps over the 2020-2050 and 2070-2100 periods, Cryosphere, 8, 1673–1697, https://doi.org/10.5194/tc-8-1673-2014, 2014.

Cogley, J., Hock, R., Rasmussen, L., Arendt, A., Bauder, A., Braithwaite, R., Jansson, P., Kaser, G., Möller, M., Nicholson, L., and Zemp, M.: Glossary of Glacier Mass Balance and Related Terms, IHP-VII Technical Documents in Hydrology No. 86, IACS Contribution No. 2, UNESCO-IHP, Paris, 2011.

Desilets, D., Zreda, M., and Ferré, T. P.: Nature's neutron probe: Land surface hydrology at an elusive scale with cosmic rays, Water Resources Research, 46, 1–7, https://doi.org/10.1029/2009WR008726, 2010.

Efthymiadis, D., Jones, P. D., Briffa, K. R., Auer, I., Böhm, R., Schöner, W., Frei, C., and Schmidli, J.: Construction of a 10-min-gridded precipitation data set for the Greater Alpine Region for 1800-2003, Journal of Geophysical Research Atmospheres, 111, 1–22, https://doi.org/10.1029/2005JD006120, 2006.

Egli, L., Jonas, T., and Meister, R.: Comparison of different automatic methods for estimating snow water equivalent, Cold Regions Science and Technology, 57, 107–115, https://doi.org/10.1016/j.coldregions.2009.02.008, 2009.

Fischer, M., Huss, M., Barboux, C., and Hoelzle, M.: The new Swiss Glacier Inventory SGI2010: relevance of using high-resolution source data in areas dominated by very small glaciers, Arctic, Antarctic, and Alpine Research, 46, 933–945, https://doi.org/10.1657/1938-4246-46.4.933, 2014.

GLAMOS: The Swiss Glaciers 1880-2016/17, Glaciological Reports No 1-138, Yearbooks of the Cryospheric Commission of the Swiss Academy of Sciences (SCNAT), published since 1964 by VAW/ ETH Zurich, https://doi.org/10.18752/glrep_series, 1881-2018.

GLAMOS: The Swiss Glaciers 2015/16-2016/17, Glaciological Reports No 137-138, Yearbooks of the Cryospheric Commission of the Swiss Academy of Sciences (SCNAT), published since 1964 by VAW/ ETH Zurich, https://doi.org/10.18752/glrep_137-138, 2018.

Goodison, B. E., Louie, P., and Yang, D.: WMO solid precipitation measurement intercomparison, Tech. Rep. 67, World Meteorological Organization, 1998.

Gottardi, F., Carrier, P., Paquet, E., and Laval, M.-T.: Le NRC: une décennie de mesures de l'équivalent en eau du manteau neigeux dans les massifs montagneux français, International Snow Science Workshop 2013, 33, 926–930, 2013.

Heilig, A., Schneebeli, M., and Eisen, O.: Upward-looking ground-penetrating radar for monitoring snowpack stratigraphy, Cold Regions Science and Technology, 59, 152–162, https://doi.org/10.1016/j.coldregions.2009.07.008, 2009.

https://doi.org/10.5194/tc-2019-106
Preprint. Discussion started: 29 May 2019

Heilig, A., Eisen, O., and Schneebeli, M.: Temporal observations of a seasonal snowpack using upward-looking GPR, Hydrological Processes, 24, 3133–3145, https://doi.org/10.1002/hyp.7749, 2010.

Howat, I. M., De La Peña, S., Desilets, D., and Womack, G.: Autonomous ice sheet surface mass balance measurements from cosmic rays, Cryosphere, 12, 2099–2108, https://doi.org/10.5194/tc-12-2099-2018, 2018.

Huss, M., Bauder, A., and Funk, M.: Homogenization of long-term mass-balance time series, Annals of Glaciology, 50, 198–206, https://doi.org/10.3189/172756409787769627, 2009.

Huss, M., Voinesco, A., and Hoelzle, M.: Implications of climate change on Glacier de la Plaine Morte, Switzerland, Geographica Helvetica, 68, 227–237, https://doi.org/10.5194/gh-68-227-2013, 2013.

Huss, M., Dhulst, L., and Bauder, A.: New long-term mass-balance series for the Swiss Alps, Journal of Glaciology, 61, 551–562, https://doi.org/10.3189/2015JoG15J015, 2015.

Isotta, F., Begert, M., and Frei, C.: Long-Term Consistent Monthly Temperature and Precipitation Grid Data Sets for Switzerland Over the Past 150 Years, Journal of Geophysical Research: Atmospheres, https://doi.org/10.1029/2018JD029910, 2019.

Isotta, F. A., Vogel, R., and Frei, C.: Evaluation of European regional reanalyses and downscalings for precipitation in the Alpine region, Meteorologische Zeitschrift, 24, 15–37, https://doi.org/10.1127/metz/2014/0584, 2014.

Jennings, K. S., Winchell, T. S., Livneh, B., and Molotch, N. P.: Spatial variation of the rain – snow temperature threshold across the Northern Hemisphere, Nature Communications, https://doi.org/10.1038/s41467-018-03629-7, 2018.

Johnson, J. B. and Schaefer, G. L.: The influence of thermal, hydrologic, and snow deformation mechanisms on snow water equivalent pressure sensor accuracy, Hydrological Processes, 16, 3529–3542, https://doi.org/10.1002/hyp.1236, 2002.

Jonas, T., Marty, C., and Magnusson, J.: Estimating the snow water equivalent from snow depth measurements in the Swiss Alps, Journal of Hydrology, 378, 161–167, https://doi.org/10.1016/j.jhydrol.2009.09.021, 2009.

Jörg-Hess, S., Griessinger, N., and Zappa, M.: Probabilistic Forecasts of Snow Water Equivalent and Runoff in Mountainous Areas*, Journal of Hydrometeorology, 16, 2169–2186, https://doi.org/10.1175/JHM-D-14-0193.1, 2015.

Kinar, N. J. and Pomeroy, J. W.: Measurement of the physical properties of the snowpack, Reviews of Geophysics, 53, 481–544, https://doi.org/10.1002/2015RG000481.Received, 2015.

Kodama, M.: Continuous Monitoring of Snow Water Equivalent Using Cosmic-Ray Neutrons, Cold Regions Science and Technology, 3, 295–303, https://doi.org/10.1016/0165-232X(80)90036-1, 1980.

Kodama, M., Kawasaki, S., and Wada, M.: A cosmic-ray snow gauge, The International Journal Of Applied Radiation And Isotopes, 26, 774–775, https://doi.org/10.1016/0020-708X(75)90138-6, 1975.

Lehning, M., Bartelt, P., Brown, B., Russi, T., Stöckli, U., and Zimmerli, M.: SNOWPACK model calculations for avalanche warning based upon a new network of weather and snow stations, Cold Regions Science and Technology, 30, 145–157, https://doi.org/10.1016/S0165-232X(99)00022-1, 1999.

Martinaitis, S. M., Cocks, S. B., Qi, Y., Kaney, B. T., Zhang, J., and Howard, K.: Understanding Winter Precipitation Impacts on Automated Gauge Observations within a Real-Time System, Journal of Hydrometeorology, 16, 2345–2363, https://doi.org/10.1175/JHM-D-15-0020.1, 2015.

Marty, C., Abegg, B., Bauder, A., Marmy, A., Lüthi, M., Bavay, M., Hauck, C., Hoelzle, M., Huss, M., Salzmann, N., Schlögl, S., Steiger, R., and Farinotti, D.: CH2014-Impacts. Toward quantitative scenarios of climate change impacts in Switzerland, chap. Cryospheric aspects of climate change - impacts on snow, ice and ski tourism, pp. 49–55, OCCR, FOEN, MeteoSwiss, C2SM, Agroscope, ProClim, 2014.

https://doi.org/10.5194/tc-2019-106
Preprint. Discussion started: 29 May 2019

MeteoSwiss: Documentation of MeteoSwiss Grid-Data Products Daily Precipitation (final analysis): RhiresD, Tech. Rep. August, https://doi.org/OFEV2014, http://www.meteoschweiz.admin.ch/web/de/services/datenportal/gitterdaten/precip/rhiresd.Par.0007.DownloadFile.tmp/proddocrhiresd.pdf, 2013.

Mizukami, N. and Perica, S.: Spatiotemporal Characteristics of Snowpack Density in the Mountainous Regions of the Western United States, Journal of Hydrometeorology, 9, 1416–1426, https://doi.org/10.1175/2008JHM981.1, 2008.

Papula, L.: Mathematische Formelsammlung: für Ingenieure und Naturwissenschaftler, Springer-Verlag, 2010, 10 edn., 2010.

Paquet, E. and Laval, M.-t.: Experience feedback and future prospects for the use of EDF ' s Cosmic-Ray Snow Gauges, Société Hydrotechnique de France - Glaciology-Nivology Section, p. 8, 2005.

Paquet, E., Laval, M.-t., Belov, A., Eroshenko, E., Kartyshow, V., Struminsky, A., and Yanke, V.: An application of cosmic-ray neutron measurements to the determination of the snow-water equivalent, in: 30th International Cosmic Ray Conference, vol. 1, pp. 761–764, https://doi.org/10.1016/0022-1694(79)90107-0, 2008.

Pirazzini, R., Leppänen, L., Picard, G., Lopez-moreno, J. I., Marty, C., Macelloni, G., Kontu, A., von Lerber, A., Tanis, C. M., Schneebeli, M., de Rosnay, P., and Arslan, A. N.: European In-Situ Snow Measurements : Practices and Purposes, Sensors, 18, 2016 (51 pp.), https://doi.org/10.3390/s18072016, 2018.

Pulwicki, A., Flowers, G. E., Radic, V., and Bingham, D.: Estimating winter balance and its uncertainty from direct measurements of snow depth and density on alpine glaciers, Journal of Glaciology, 64, 781–795, https://doi.org/10.1017/jog.2018.68, 2018.

Raleigh, M. S. and Small, E. E.: Snowpack density modeling is the primary source of uncertainty when mapping basin-wide SWE with lidar, Geophysical Research Letters, 44, 3700–3709, https://doi.org/10.1002/2016GL071999, 2017.

Rasmussen, R., Baker, B., Kochendorfer, J., Meyers, T., Landolt, S., Fischer, A. P., Black, J., Thériault, J. M., Kucera, P., Gochis, D., Smith, C., Nitu, R., Hall, M., Ikeda, K., and Gutmann, E.: How well are we measuring snow: The NOAA/FAA/NCAR winter precipitation test bed, Bulletin of the American Meteorological Society, 93, 811–829, https://doi.org/10.1175/BAMS-D-11-00052.1, 2012.

Saito, K., Yamaguchi, S., Iwata, H., Harazono, Y., Kosugi, K., Lehning, M., and Shulski, M.: Climatic physical snowpack properties for large-scale modeling examined by observations and a physical model, Polar Science, 6, 79–95, https://doi.org/10.1016/j.polar.2012.02.003, 2012.

Schattan, P., Baroni, G., Oswald, S. E., Schöber, J., Fey, C., Kormann, C., Huttenlau, M., and Achleitner, S.: Continuous monitoring of snowpack dynamics in alpine terrain by aboveground neutron sensing, Water Resources Research, 53, 3615–3634, https://doi.org/10.1002/2016WR020234, 2017.

Schmid, L., Heilig, A., Mitterer, C., Schweizer, J., Maurer, H., Okorn, R., and Eisen, O.: Continuous snowpack monitoring using upward-looking ground-penetrating radar technology, Journal of Glaciology, 60, 509–525, https://doi.org/10.3189/2014JoG13J084, 2014.

Schmid, L., Koch, F., Heilig, A., Prasch, M., Eisen, O., Mauser, W., and Schweizer, J.: A novel sensor combination (upGPR-GPS) to continuously and nondestructively derive snow cover properties, Geophysical Research Letters, pp. 3397–3405, https://doi.org/10.1002/2015GL063732, 2015.

Sevruk, B., Ondrás, M., and Chvíla, B.: The WMO precipitation measurement intercomparisons, Atmospheric Research, 92, 376–380, https://doi.org/10.1016/j.atmosres.2009.01.016, 2009.

Sigouin, M. J. P. and Si, B. C.: Calibration of a non-invasive cosmic-ray probe for wide area snow water equivalent measurement, The Cryosphere, 10, 1181–1190, https://doi.org/10.5194/tc-2015-216, 2016.

Sims, E. M. and Liu, G.: A parameterization of the orobability of snow–rain transition, Journal of Hydrometeorology, 16, 1466–1477, https://doi.org/10.1175/jhm-d-14-0211.1, 2015.

https://doi.org/10.5194/tc-2019-106
Preprint. Discussion started: 29 May 2019

SLF Data: Automatic snow stations from the Intercantonal Measurement and Information System (IMIS), WSL Institute for Snow and Avalanche Research SLF. Davos, Switzerland, 2015.

Sold, L., Huss, M., Hoelzle, M., Andereggen, H., Joerg, P. C., and Zemp, M.: Methodological approaches to infer end-of-winter snow distribution on alpine glaciers, Journal of Glaciology, 59, 1047–1059, https://doi.org/10.3189/2013JoG13J015, 2013.

Sold, L., Huss, M., Machguth, H., Joerg, P. C., Leysinger Vieli, G., Linsbauer, A., Salzmann, N., Zemp, M., and Hoelzle, M.: Mass Balance Re-analysis of Findelengletscher, Switzerland; Benefits of Extensive Snow Accumulation Measurements, Frontiers in Earth Science, 4, 18, https://doi.org/10.3389/feart.2016.00018, https://www.frontiersin.org/article/10.3389/feart.2016.00018, 2016.

Sorteberg, H. K., Engeset, R. V., and Udnæs, H. C.: A national network for snow monitoring in Norway: Snow pillow verification using observations and models, Physics and Chemistry of the Earth, Part C: Solar, Terrestrial and Planetary Science, 26, 723–729, https://doi.org/10.1016/S1464-1917(01)95016-0, 2001.

Steiner, L., Meindl, M., Fierz, C., and Geiger, A.: An assessment of sub-snow GPS for quantification of snow water equivalent, The Cryosphere, 12, 3161–3175, https://doi.org/10.5194/tc-12-3161-2018, 2018.

Stuefer, S., Kane, L. D., and Liston, G. E.: In situ snow water equivalent observations in the U . S . Arctic, Hydrology Research, 44, 21–34, https://doi.org/10.2166/nh.2012.177, 2013.

Sturm, M., Goldstein, M. A., and Parr, C.: Water and life from snow: A trillion dollar science question, Water Resources Research, pp. 3534–3544, https://doi.org/10.1002/2017WR020840.Received, 2017.

Thibert, E., Blanc, R., Vincent, C., and Eckert, N.: Glaciological and volumetric mass-balance measurements: Error analysis over 51 years for Glacier de Sarennes, French Alps, Journal of Glaciology, 54, 522–532, https://doi.org/10.3189/002214308785837093, 2008.

Viviroli, D., Dürr, H. H., Messerli, B., Meybeck, M., and Weingartner, R.: Mountains of the world, water towers for humanity: Typology, mapping, and global significance, Water Resources Research, 43, W07 447, https://doi.org/10.1029/2006WR005653, 2007.

Viviroli, D., Archer, D. R., Buytaert, W., Fowler, H. J., Greenwood, G. B., Hamlet, A. F., Huang, Y., Koboltschnig, G., Litaor, M. I., López-Moreno, J. I., Lorentz, S., Schädler, B., Schreier, H., Schwaiger, K., Vuille, M., and Woods, R.: Climate change and mountain water resources: Overview and recommendations for research, management and policy, Hydrology and Earth System Sciences, 15, 471–504, https://doi.org/10.5194/hess-15-471-2011, 2011.

Zreda, M., Desilets, D., Ferré, T. P. A., and Scott, R. L.: Measuring soil moisture content non-invasively at intermediate spatial scale using cosmic-ray neutrons, Geophysical Research Letters, 35, https://doi.org/10.1029/2008GL035655, 2008.

Zreda, M., Shuttleworth, W. J., Zeng, X., Zweck, C., Desilets, D., Franz, T., and Rosolem, R.: COSMOS: The cosmic-ray soil moisture observing system, Hydrology and Earth System Sciences, 16, 4079–4099, https://doi.org/10.5194/hess-16-4079-2012, 2012.